physica status solidi b

phys. stat. sol. (b) **244**, No. 11, 4006–4010 (2007) / **DOI** 10.1002/pssb.200776141

First and second optical transitions in single-walled carbon nanotubes: a resonant Raman study

H. Telg[*, 1], **J. Maultzsch**[**, 1], **S. Reich**[2], and **C. Thomsen**[1]

[1] Institut für Festkörperphysik, Technische Universität Berlin, Hardenbergstr. 36, 10623 Berlin, Germany
[2] Department of Materials Science and Engineering, Massachusetts Institute of Technology, 77 Massachusetts Avenue, Cambridge, Massachusetts 02139-4307, USA

Received 17 May 2007, revised 6 July 2007, accepted 6 July 2007
Published online 8 October 2007

PACS 63.22.+m, 73.22.–f, 78.30.Na, 78.67.Ch, 81.07.De

Resonant Raman spectroscopy was performed to study electron–phonon coupling in single-walled carbon nanotubes separated in solution. By varying the excitation energy from 1.26 eV to 1.93 eV we obtained radial breathing mode resonance profiles of the first and second optical transitions E_{11} and E_{22} of the (9,1) and (8,3) tubes. We observe up to 16 times stronger Raman intensities for the E_{11} transitions which can mostly be attributed to a two times broader linewidth of the E_{22} transition. Comparison of the matrix element ratio $\mathcal{M}_{11}/\mathcal{M}_{22}$ to theoretical predictions on the electron–phonon coupling show a deviation of a factor 1.7 which might be associated with the change of the exciton–photon matrix element.

1 Introduction

Raman spectroscopy plays an important part in the research of carbon nanotubes. It is used to distinguish metallic from semiconducting tubes [1] and for probing the diameter distribution in a sample [2]. Resonant Raman scattering even enables the determination of the chiral indices (n_1,n_2) of nanotubes present in a sample [3, 4]. Despite the wide use of this technique there remains a lack of knowledge about the Raman cross section. The fact that the cross section of the radial breathing mode (RBM) strongly depends on the chiral indices makes the determination of chiral abundances, which is crucial regarding selective growth and (n_1,n_2) separation, very difficult.

The first approaches to measure the Raman cross section of the RBM in carbon nanotubes was to collect resonance profiles and to determine the maximum Raman intensities [5–8]. To obtain the relative cross sections it was necessary to assume a uniform diameter distribution. More recently Yin et al. [9] and Shreve et al. [10] determined the electron–phonon matrix elements by measuring the Raman intensities of the first and second order RBM. This technique is free of assumptions concerning chiral index distributions in a given sample but depends on the phonon dispersion, which is based on predictions. Detailed theoretical predictions on the electron–phonon coupling strength or the Raman intensity were realized using *ab initio* [11] or modified tight-binding models [8, 12, 13] including excitonic effects in more recent work [13]. To compare theoretical predictions to experimental results we looked for experimental values which are independent on prior assumptions about the (n_1,n_2) distribution. Raman intensities excited resonantly into the first and second optical transitions of nanotubes with the same chiral index (n_1,n_2) provide a basis for such a comparison.

[*] Corresponding author: e-mail: telg@physik.tu-berlin.de, Phone: +49 30 314 22 083, Fax: +49 30 314 27 705
[**] Present address: Dept. of Electrical Engineering, Columbia University, New York, NY 10027, USA

In this paper we report on Raman measurements of the radial breathing mode of nanotubes separated in solution. We compared Raman intensities of particular semiconducting nanotubes when exciting resonantly into the first and second optical transition. We observe an up to 16 times stronger signal when exciting resonantly into the first transition. It can be shown that this difference is mainly due to different lifetimes of E_{11} and E_{22}. We find that the Raman matrix elements are similar for E_{11} and E_{22}. By comparison to theoretical predictions of the electron–phonon coupling ratio $\mathcal{M}_{11}/\mathcal{M}_{22}$ we find the results to deviate by a factor of 1.7. One possible explanation for this deviation is a 1.3 times larger exciton–photon coupling in case of the E_{11} transition than in E_{22}.

2 Experimental

We performed resonant Raman spectroscopy on single-walled carbon nanotubes ultrasonically dispersed in D_2O. To prevent the HiPCO-type nanotubes from rebundling they were enclosed in sodium dodecyl sulfate micelles [14]. Using tunable laser systems we varied the excitation energy from 1.26 eV to 1.46 eV and from 1.72 eV to 1.93 eV. These energy regions were chosen in order to resonantly excite the first and second optical transition of the (9,1) and (8,3) nanotube [6]. Stokes and anti-Stokes radial breathing mode spectra were collected using a Dilor XY800 triple-monochromator setup in backscattering geometry. Subsequently spectra were normalized to the intensity of the Raman signal from CaF_2 (326 cm^{-1}), the Bose–Einstein occupation number and the inverse phonon energy. After this normalization the measured Raman intensities are proportional to the square of the Raman susceptibility.

3 Results and discussion

In Fig. 1 we show four contour plots with the corrected Raman intensities as a function of excitation energy and Raman shift. In each plot the resonances of the RBM of a number of tubes appear. By comparison to recent work it can be shown that each plot contains the resonance of at least the (9,1) and the

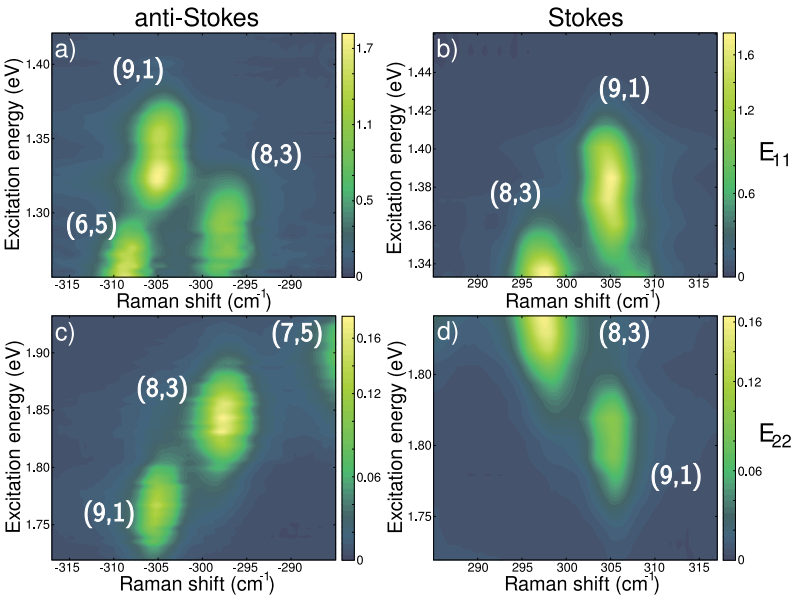

Fig. 1 (online colour at: www.pss-b.com) Contour plots of the RBM spectra normalized as described in the text. The plotted intensities are proportional to the Raman susceptibility. Upper plots contain anti-Stokes (a) and Stokes (b) Raman spectra excited resonantly via E_{11}. Lower plots show anti-Stokes (c) and Stokes (d) spectra in resonance with E_{22}.

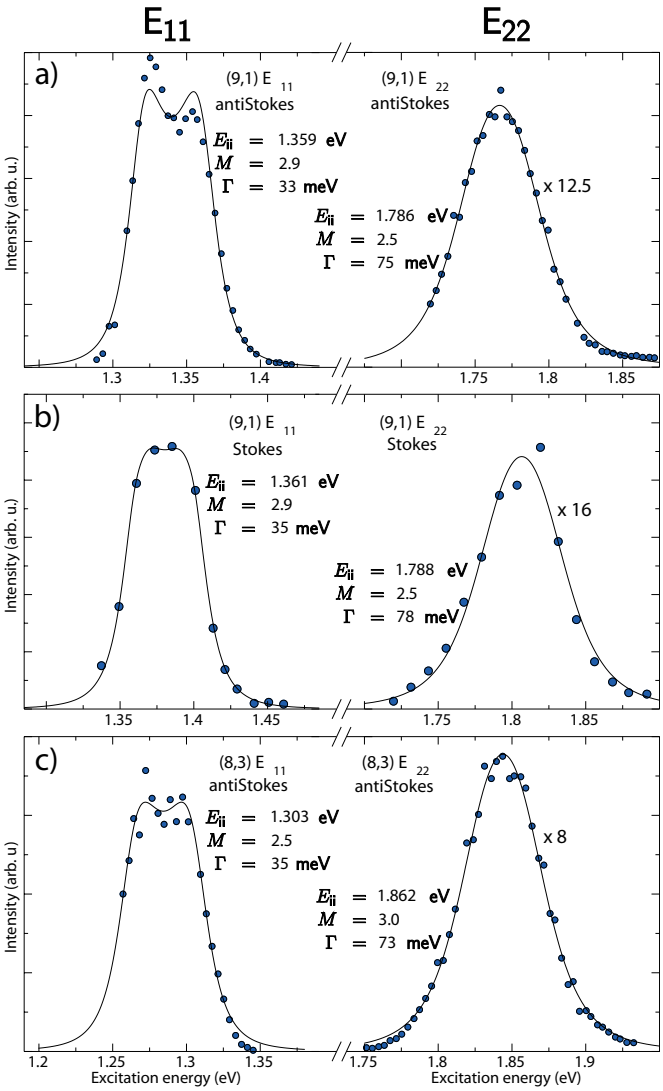

Fig. 2 (online colour at: www.pss-b.com) RBM resonance profiles of the E_{11} (left) and the E_{22} (right) transition for two nanotube types, the (9,1) anti-Stokes (a) and Stokes (b), and the (8,3) anti-Stokes (c). Intensities of the E_{22} resonance profiles are scaled by the given factor with respect to the corresponding E_{11} profiles. For better comparability the width of the energy intervals is the same for all plots. Graphs are the best fits of Eq. (1) to the experimental data. Fitresults are given in each plot. M is proportional to $\mathcal{M}$ including the remaning constants c.

(8,3) nanotubes [5, 6], see labels in the figure. While plot (a) and (b) show the anti-Stokes and Stokes spectra with resonant excitation into the first optical transitions (E_{11}), plot (c) and (d) show the anti-Stokes and Stokes spectra when exciting resonantly into the second optical transitions (E_{22}). In order to gain resonance profiles we fitted each RBM with a Lorentzian profile. Plotting the area of the Lorentzian as a function of excitation energy E_{laser} yields a resonance profile as shown in Fig. 2.

In Fig. 2 we compare the resonance profiles of the E_{11} (left) and the E_{22} (right) of the (9,1) and (8,3) nanotube. At first glance the large intensity difference between the first and second transition is apparent. The maximum Raman intensities of the E_{11} transitions are up to 16 times larger than the intensities of the

corresponding E_{22} transitions. From this result one might be tempted to deduce a stronger electron–phonon–coupling or absorption in case of E_{11}. An indication that this is not the case is given by the slopes of the resonance profiles. Obviously the slopes of the E_{11} resonance profiles are much steeper than those of the E_{22} profiles (the relative scale of the energy axes is the same for all plots in Fig. 2). This corresponds to a change in the line width of the underlying electronic transition. In order to extract the linewidth Γ and the matrix elements ($\mathcal{M}$) of the absorption and the electron–phonon coupling we fit the following expression to the resonance profiles [15],

$$I(E_{\text{laser}}) = \frac{c}{E_{\text{laser}}^2} \cdot \frac{|\mathcal{M}|^2}{[(E_{\text{laser}} - E_{ii})^2 + \Gamma^2/4][(E_{\text{laser}} - \hbar\omega - E_{ii})^2 + \Gamma^2/4]}. \quad (1)$$

Fitting with this expression also yields the transition energy E_{ii}, where *ii* denotes the involved subbands, $\hbar\omega$ is the phonon energy, and c contains remaining constants. The fit results (Fig. 2) show that in fact the Raman matrix elements $\mathcal{M}$ of E_{11} and E_{22} are similar. The strong intensity difference is mainly due to the change in Γ, which is approximately twice as large for E_{22} as for E_{11}. Γ is the imaginary part of the electronic transition energy E_{ii} and thus related to the lifetime of the transition. The observed change in Γ can be interpreted as longer lifetimes of excitations in the first excitonic state – a result which is also known from time resolved measurements [16]. We do not give absolute values for the lifetime since a is affected by inhomogeneities in the sample like the formation of small bundles and varying tube length. Differences in the sample quality might also be the reason for deviations between our results and result from Satishkumar et al. [8]. They observed twice larger intensity ratios I_{11}/I_{22} and an accordingly smaller line width of E_{11}. Interestingly, their values for Γ of the second optical transitions do not differ significantly from our results. Apparently the (shorter) lifetime of the E_{22}-exciton is much less affected by environmental changes.

In the following section we compare our results to predictions from theory. Most publications which provide theoretical predictions of Raman intensities or electron–phonon coupling strength are based on the free-particle picture, so they do not include excitonic effects [11, 12]. In Ref. [13] the Raman intensities are calculated including excitonic effects, however, only results on E_{22} are given. The authors of Ref. [13] show that the exciton–photon matrix element $\mathcal{M}_{\text{ex-op}}$ depends only on diameter, not on chiral angle. Therefore we can assume the ratio $\mathcal{M}^{11}_{\text{ex-op}}/\mathcal{M}^{22}_{\text{ex-op}}$ to be approximately constant at least for a limited diameter range. Second, the behavior of the exciton–phonon matrix elements $\mathcal{M}_{\text{ex-ph}}$ in Ref. [13] shows hardly any deviation from results based on the free-particle picture. With these assumptions we compare our experimental results on the matrix elements ($\mathcal{M} = \mathcal{M}^2_{\text{ex-op}}\,\mathcal{M}_{\text{ex-ph}}$) to predictions on the electron–phonon coupling strength based on the free-particle picture. Deviations might then be associated to changes in the exciton–photon coupling between E_{11} and E_{22}.

Popov et al. [12] calculated Raman intensities of E_{11} and E_{22} for a large number of chiral indices (n_1, n_2) using a nonorthogonal tight-binding model in the free-particle picture. In order to compare our results to those in Ref. [12] we calculated the ratio of the electron–phonon matrix elements from Ref. [12] $\mathcal{M}^{11}_{\text{el-ph}}/\mathcal{M}^{22}_{\text{el-ph}}$ and from the matrix elements resulting from our measurements $\mathcal{M}_{11}/\mathcal{M}_{22}$. In case of the (9,1) nanotube this ratio is 0.65 which is 1.76 times smaller than our experimental result (1.14). For the (8,3) $\mathcal{M}^{11}_{\text{el-ph}}/\mathcal{M}^{22}_{\text{el-ph}}$ is 0.50, which is 1.67 times smaller than our result (0.8). For both nanotubes $\mathcal{M}^{11}_{\text{el-ph}}/\mathcal{M}^{22}_{\text{el-ph}}$ is ≈1.7 times larger in the experimental results than predicted. One possible explanation is that the deviation is due to changes in the exciton–photon matrix elements $\mathcal{M}^{ii}_{\text{ex-op}}$. This would imply a ratio $\mathcal{M}^{11}_{\text{ex-op}}/\mathcal{M}^{22}_{\text{ex-op}}$ of 1.3 ($\sqrt{1.7}$).

4 Conclusion

We studied the Raman intensities exciting resonantly into the first and second optical transitions. We observed strong intensity differences between the two transitions which are mostly due to the smaller linewidth of the E_{11} transition. Comparison to results from Ref. [8] show deviations only in the linewidth of E_{11} implying this transition to be more sensitive to environmental effects. We find that the matrix

elements vary only slightly between E_{11} and E_{22}. By comparing the ratio of the matrix elements to theoretical predictions on the electron–phonon coupling we find a deviation of 1.7, which might be associated with a 1.3 times larger exciton–photon coupling for E_{11} compared to E_{22}.

Acknowledgements We thank F. Hennrich for providing us with the samples. J.M. acknowledges support from the Alexander-von-Humboldt foundation.

References

[1] M. A. Pimenta, A. Marucci, S. A. Empedocles, M. G. Bawendi et al., Phys. Rev. B **58**, R16016 (1998).
[2] A. M. Rao, E. Richter, S. Bandow, B. Chase, P. C. Eklund et al., Science **275**, 187 (1997).
[3] H. Telg, J. Maultzsch, S. Reich, F. Hennrich, and C. Thomsen, Phys. Rev. Lett. **93**, 177401 (2004).
[4] C. Fantini, A. Jorio, M. Souza, M. S. Strano et al., Phys. Rev. Lett. **93**, 147406 (2004).
[5] J. Maultzsch, H. Telg, S. Reich, and C. Thomsen, Phys. Rev. B **72**, 205438 (2005).
[6] H. Telg, J. Maultzsch, S. Reich, and C. Thomsen, Phys. Rev. B **74**, 115415 (2006).
[7] S. K. Doorn, D. A. Heller, P. W. Barone, M. L. Usrey, and M. S. Strano, Appl. Phys. A **78**, 1147 (2004).
[8] B. C. Satishkumar, S. V. Goupalov, E. H. Haroz, and S. K. Doorn, Phys. Rev. B **74**, 155409 (2006).
[9] Y. Yin, A. N. Vamivakas, A. G. Walsh, S. B. Cronin, M. S. Ünlü, B. B. Goldberg, and A. K. Swan, Phys. Rev. Lett. **98**, 037404 (2007).
[10] A. P. Shreve, E. H. Haroz, S. M. Bachilo, R. B. Weisman, S. Tretiak, S. Kilina, and S. K. Doorn, Phys. Rev. Lett. **98**, 037405 (2007).
[11] M. Machón, S. Reich, H. Telg, J. Maultzsch, P. Ordejón, and C. Thomsen, Phys. Rev. B **71**, 035416 (2005).
[12] V. N. Popov, L. Henrard, and P. Lambin, Phys. Rev. B **72**, 035436 (2005).
[13] J. Jiang, R. Saito, K. Sato, J. S. Park, G. G. Samsonidze et al., Phys. Rev. B **75**, 035405 (2007).
[14] S. Lebedkin, F. Hennrich, T. Skipa, and M. M. Kappes, J. Phys. Chem. B **107**, 1949 (2003).
[15] C. Thomsen and S. Reich, in: Light Scattering in Solids IX, Topics in Applied Physics, Vol. 108, edited by M. Cardona and R. Merlin (Springer, Berlin, 2007).
[16] J.-S. Lauret, C. Voisin, G. Cassabois, C. Delalande, P. Roussignol, O. Jost, and L. Capes, Phys. Rev. Lett. **90**, 057404 (2003).

